

Antarctic last interglacial isotope peak in response to sea ice retreat not ice-sheet collapse

Article

Accepted Version

Holloway, M. D., Sime, L. C., Singarayer, J. S., Tindall, J. C., Bunch, P. and Valdes, P. J. (2016) Antarctic last interglacial isotope peak in response to sea ice retreat not ice-sheet collapse. *Nature Communications*, 7. 12293. ISSN 2041-1723 doi: <https://doi.org/10.1038/ncomms12293> Available at <https://centaur.reading.ac.uk/66728/>

It is advisable to refer to the publisher's version if you intend to cite from the work. See [Guidance on citing](#).

Published version at: <http://dx.doi.org/10.1038/ncomms12293>

To link to this article DOI: <http://dx.doi.org/10.1038/ncomms12293>

Publisher: Nature Publishing Group

All outputs in CentAUR are protected by Intellectual Property Rights law, including copyright law. Copyright and IPR is retained by the creators or other copyright holders. Terms and conditions for use of this material are defined in the [End User Agreement](#).

www.reading.ac.uk/centaur

CentAUR

Central Archive at the University of Reading

Reading's research outputs online

Antarctic last interglacial isotope peak in response to sea ice retreat not ice sheet collapse

Max D Holloway^{*1,2}, Louise C Sime¹, Joy S Singarayer³, Julia C Tindall⁴,

Pete Bunch⁵ & Paul J Valdes²

¹Ice Dynamics and Paleoclimate, British Antarctic Survey, Cambridge, UK, CB3 0ET

²School of Geographical Sciences, University of Bristol, Bristol, UK, BS8 1SS

³Department of Meteorology, University of Reading, Reading, UK, RG6 6BB

⁴School of Earth and Environment, University of Leeds, Leeds, UK, LS2 9JT

⁵Department of Engineering, University of Cambridge, Cambridge, UK, CB2 1PZ

*To whom correspondence should be addressed; E-mail: mh12534@bristol.ac.uk.

Several studies have suggested that sea level rise during the last interglacial implies retreat of the West Antarctic Ice Sheet (WAIS). The prevalent hypothesis is that the retreat coincided with the peak Antarctic temperature and stable water isotope values from 128,000 years ago (128 ka); very early in the last interglacial. Here, by analysing the first ever climate model simulations of last interglacial WAIS loss featuring water isotopes, we show instead that the isotopic response to WAIS loss is in opposition to the isotopic evidence at 128 ka. Instead, a reduction in winter sea ice area of 65 ± 7 % fully explains the 128 ka ice core evidence. Our finding of a dramatic retreat of the sea ice at 128 ka demonstrates, for the first time, the sensitivity of Antarctic sea ice extent to climate warming.

1 Introduction

During the last interglacial (LIG; 130,000 to 115,000 years ago) global climate was warmer than today¹⁻⁴ and global mean sea level was 6-9 m higher⁵⁻¹⁰ (Fig. 1). This LIG sea level high stand was

mainly driven by ice sheet loss^{5,11}. Recent ice core results indicate that the Greenland Ice Sheet likely provided a modest 2 m contribution towards the global sea level rise⁵, with estimates ranging from +1.4 m to +4.3 m¹². This implies that ice loss from the West Antarctic Ice Sheet (WAIS) must have contributed to the LIG sea level maxima: loss of the entire WAIS would contribute 3-4 m of global sea level rise^{13,14}. Coral records from Western Australia indicate that sea level rose late in the interglacial, around 118,000 years ago (118 ka)⁹. However, Seychelles coral has been interpreted as indication of a +5 m global sea level at 128 ka⁶. These differing interpretations prevent constraint on the timing of WAIS loss, thus reducing the potential to use the LIG to inform the debate on the likelihood of future WAIS loss^{11,13,14}. We therefore turn to the ice core records to push forward the WAIS loss debate.

The recent ice core drilled at WAIS Divide¹⁵ does not extend back through the LIG; ice that may have been present during the LIG has since been lost through basal melt. However, ice cores extending back throughout the LIG, at a resolution of less than 200 years per m of ice¹⁶, are available from four locations on the East Antarctic Ice Sheet (Fig. 1). From west to east these are: EPICA Dronning Maud Land (EDML); Dome F (DF); Vostok; and EPICA Dome C (EDC). These four ice cores all record an isotopic maximum at approximately 128 ka, associated with peak Antarctic warmth^{1,17,18}. Relative to the last 3 ka this LIG isotopic maximum is between 2 and 4 ‰ in $\delta^{18}\text{O}$. It has been suggested that WAIS loss is required to explain the magnitude of this isotope maximum^{2,19}.



We carry out a series of climate model experiments incorporating $\delta^{18}\text{O}$ ²⁰ (see Methods for full details). All experiments are forced by 128 ka orbital and greenhouse gas concentrations and compared to a pre-industrial control simulation. These experiments test whether loss of the WAIS was responsible for the 128 ka isotopic anomaly. Three suites of experiments are performed. The first experiment is forced by 128 ka orbital and greenhouse gas forcing alone. This experiment uses

a modern WAIS volume and shape. The second suite comprises three experiments using alternative versions of the WAIS (Supplementary Figure 1): a remnant flat WAIS, at an elevation of 200 m¹⁹; the entire WAIS removed, and the exposed (submerged) bedrock replaced with a new region of ocean; and the WAIS removed and replaced with ocean but with isotopically depleted freshwater, melted from the WAIS, allowed to enter the Southern Ocean. To our knowledge these are the first isotope-enabled, coupled atmosphere-ocean global climate model simulations in which the WAIS has been removed and inundated with ocean. The third suite of experiments explores an alternative hypothesis; that reduced Southern Hemisphere sea ice extent provides an alternative explanation for the 128 ka isotopic maximum^{15,21–23}. Both ice and ocean core evidence suggests that a large retreat of the Antarctic sea ice edge may have occurred at 128 ka^{22–24}. This third suite of sea ice reduction experiments are performed using both a modern WAIS configuration and with the WAIS removed (but with no additional meltwater added to the Southern Ocean). See Supplementary Table 1 for a full list of experiments.

Our results suggest that a full WAIS collapse cannot explain the magnitude or the spatial pattern of the 128 ka $\delta^{18}\text{O}$ maximum. Removing the WAIS causes changes in atmospheric circulation and precipitation seasonality which tends to reduce $\delta^{18}\text{O}$. Including WAIS meltwater reduces $\delta^{18}\text{O}$ by freshening the surface ocean, resulting in cooling and sea ice expansion, which does not improve the model-data agreement. A major sea ice retreat of $65 \pm 7\%$ increases $\delta^{18}\text{O}$ and does result in a good model-data agreement. This finding will have consequences for sea ice projection in a future warmer climate.

2 Results

128 ka simulations with changes in WAIS morphology. The isotopic response to 128 ka orbital and greenhouse gas forcing alone (and no change in WAIS morphology) is weak (Fig. 2a). Simu-

lated $\delta^{18}\text{O}$ anomalies at the ice core sites range between -1.55 and +0.26 ‰. When the response to a remnant 200 m WAIS is simulated, $\delta^{18}\text{O}$ anomalies at the ice core sites range from -0.18 to +0.96 ‰ (Fig. 2b); and when the WAIS is fully removed and new ocean regions created, the simulated $\delta^{18}\text{O}$ anomalies become further depleted to between -2.78 and +0.63 ‰ (Fig. 2c). Simulated $\delta^{18}\text{O}$ anomalies are strongly positive over the WAIS for all experiments with a reduced WAIS. Reduced elevation increases surface air temperature at a rate roughly proportional to the lapse rate ($\sim 6^\circ\text{C km}^{-1}$; see Supplementary Figure 2), which in turn enriches the isotopic composition of local vapour. If we include the effects of meltwater from a WAIS collapse, the $\delta^{18}\text{O}$ depletion becomes more pronounced (Fig. 2d). A reduction in the Southern Ocean source water $\delta^{18}\text{O}$ alongside an expansion in sea ice both tend to reduce $\delta^{18}\text{O}$ at the ice core sites. These simulated $\delta^{18}\text{O}$ results, from each of our three WAIS loss scenarios, do not match the 128 ka $\delta^{18}\text{O}$ values from the ice core data.

Decomposition of changes in $\delta^{18}\text{O}$. At the ice core sites, changes in both the isotopic composition and the seasonality of precipitation contribute to the simulated negative $\delta^{18}\text{O}$ anomalies. Although the precipitation over the ice core sites tends to be enriched during colder months due to WAIS loss, an increased proportion of precipitation falling during colder months leads to an overall depletion of $\delta^{18}\text{O}$ (Supplementary Figures 3 and 4).

To qualify the relative impact of precipitation and $\delta^{18}\text{O}$ seasonality, we first isolate the changes in $\delta^{18}\text{O}$ due to changes in the seasonal cycle of precipitation (ΔP_{seas})²⁵;

$$\Delta P_{seas} = \frac{\sum_j \delta^{18}\text{O}_j^{MOD} \cdot P_j}{\sum_j P_j} - \frac{\sum_j \delta^{18}\text{O}_j^{MOD} \cdot P_j^{MOD}}{\sum_j P_j^{MOD}} \quad (1)$$

Superscript ^{MOD} indicate values from the 128 ka experiment using a modern WAIS configuration and no superscript indicate values from the WAIS sensitivity experiments. The difference between the total $\delta^{18}\text{O}$ change ($\Delta\delta^{18}\text{O}$) and ΔP_{seas} represents other effects contributing to the observed

$\delta^{18}\text{O}$ anomaly (such as variability in the $\delta^{18}\text{O}$ of precipitate and in the source vapour);

$$\Delta_{\delta} = \Delta\delta^{18}\text{O} - \Delta P_{seas} \quad (2)$$

For all WAIS retreat scenarios (a remnant WAIS, WAIS removed and replaced with ocean, and WAIS removed and meltwater added to the Southern Ocean) ΔP_{seas} is negative; a larger proportion of precipitation falls on the EAIS during cold months when the WAIS is absent (Fig. 3, middle panels). This differs from the WAIS loss experiments of Holden *et al.*¹⁹, who observe an increase in summer precipitation. This discrepancy is likely explained by differences in the modelling set-up; Holden *et al.* include different boundary forcing (chosen for 130 ka), the WAIS replaced by “ice-free” land at an elevation of 200m, and 1 Sv of freshwater added to the North Atlantic.

Changes in Δ_{δ} are strongly positive over the WAIS for all experiments with a reduced WAIS, which is a direct response to the lowered elevation and associated warming, mentioned above (Fig. 3, right panels). The response of Δ_{δ} over the EAIS differs between the WAIS retreat scenarios. Δ_{δ} is positive over the EAIS for a remnant flat WAIS but turns negative when the WAIS is removed and replaced with ocean. This suggests that there are changes in the intensity of precipitation falling over the EAIS and/or a change in precipitation source region when the WAIS is replaced with ocean. Such changes in the amount and/or intensity of precipitation over Antarctica would be consistent with the expected changes in the thermal characteristics of the high southern latitudes; lower Antarctic Ice Sheet (AIS) topography has been linked with intensified cyclones over the continent (suppressed for higher AIS)²⁶. These changes allow more storms to travel over the continent, which are a key mechanism for transporting moisture inland²⁶.

When the WAIS is replaced with ocean and meltwater is added to the Southern Ocean, Δ_{δ} is negative everywhere apart from the elevation induced positive anomalies over the WAIS (Fig. 3i). This is a response to the depleted isotopic composition of the prescribed meltwater (-30 ‰), depleting the isotopic composition of the surface Southern Ocean that is a source for Antarctic

precipitation, and a freshwater associated expansion in Southern Hemisphere sea ice.

128 ka simulations with WAIS and sea ice retreat. Sea ice retreat in the presence and absence of the WAIS both enrich $\delta^{18}\text{O}$ at the ice core sites. Water vapour becomes relatively enriched in heavy isotopes in response to evaporative input from new water surfaces exposed by the retreat of sea ice. A reduced distance between evaporation source and precipitation site for atmospheric water vapour tends to enrich $\delta^{18}\text{O}^{21}$. However, there are considerable differences across East Antarctica in the $\delta^{18}\text{O}$ response to WAIS presence and WAIS loss. Following a Bayesian analysis, we assess which of these scenarios best explains the observed data (see Methods for details). Our results strongly support the conclusion that the WAIS was present at 128 ka. Comparing the two scenarios using a statistical model comparison, the likelihood ratio is 200 in favour of the WAIS being present, i.e. the observations are 200 times more likely using a model with the WAIS present than when the WAIS is removed. The WAIS-removed scenario does not explain the observed spatial pattern of $\delta^{18}\text{O}$ measurements as well as the model simulations that retain the WAIS.

When the WAIS is present, a winter (September) sea ice area reduction of 65 % (posterior mean with a 95 % credibility interval of 58 to 72 %) relative to pre-industrial provides a data-model match of better than ± 0.02 ‰ with the $\delta^{18}\text{O}$ anomaly at Vostok and EDML, better than ± 0.8 ‰ at EDC and ± 1.1 ‰ at Dome F (Fig. 4a and 5). With the WAIS removed, the best fit to the ice core observations is similarly achieved with a sea ice reduction of 66 %. However, the uncertainty band is nearly four times larger (95 % credible interval of 32 to 87 %) and the model-data match is worse at every site; the model-data $\delta^{18}\text{O}$ match is worse than ± 0.05 ‰ at EDML, ± 1.0 ‰ at Vostok, ± 1.9 ‰ at EDC and ± 3.5 ‰ at Dome F (Fig. 4b). This multi-ice core data-model comparison thus suggests that complete loss of the WAIS at 128 ka is inconsistent with the ice core evidence.


3 Discussion

We have explored only complete WAIS loss, rather than WAIS reduction, scenarios here. Our results thus do not preclude some loss of the WAIS by 128 ka, or that the WAIS may have been lost later in the LIG, possibly preconditioned by the early retreat of Southern Hemisphere sea ice. Indeed, loss of the WAIS between 128 and 125 ka and a meltwater driven build up of Southern Hemisphere sea ice may provide an explanation for the late LIG $\delta^{18}\text{O}$ drop observed in ice core records; the $\delta^{18}\text{O}$ trend throughout the early LIG, with a significant peak and subsequent drop, is distinct from the isotope record of the present interglacial (Fig. 1). Our results indicate that the LIG isotope trend may be consistent with a WAIS collapse and sea ice build up in the following few thousand years of the isotope maximum.

The difference between an isotope record from Mt. Moulton and East Antarctic ice core records²⁷ may also be consistent with a slow loss of the WAIS, which could have been mostly melted after another 2,000 years, by around 126 ka. Lower isotope anomalies in the Mt. Moulton record relative to isotope records from East Antarctica suggest a local cooling anomaly, which is consistent with climate model simulations of WAIS collapse driven by pre-industrial boundary conditions²⁷. The low isotope values in the Mt. Moulton record, relative to the other ice core sites, persists throughout the LIG, but the difference is greatest after ~ 126 ka, perhaps coinciding with maximum retreat of the WAIS. Considering the reasonable agreement between the observed peak-to-trough $\delta^{18}\text{O}$ anomalies and those calculated between our sea ice retreat and the WAIS loss experiments (Supplementary Figure 5), we suggest that a large sea ice retreat best explains the early isotope maximum and a subsequent retreat of the WAIS and sea ice build-up could provide an explanation for the observed pattern of isotope anomalies following the LIG maximum.

The bipolar seesaw mechanism²⁸ proposes that a slowdown in northwards ocean heat transport, particularly in the Atlantic, tends to warm the Southern Ocean. This mechanism is consistent

with a recent bipolar re-interpretation of the early LIG²⁹, alongside a recent synthesis of sea surface temperature reconstructions between 40 and 60 °S⁴. These all support Southern Ocean warming at 128 ka; providing a partial explanation for why Southern Hemisphere sea ice retreated at 128 ka. In future work, we will investigate whether the bipolar-seesaw can provide the mechanism to cause a major Southern Hemisphere sea ice retreat and thus reconcile the 128 ka $\delta^{18}\text{O}$ maximum. Further simulations, including WAIS loss and North Atlantic meltwater input, could provide insight into the non-linear interactions between the bipolar-seesaw, the WAIS and Southern Hemisphere sea ice.

Finally, we note the similarity between the wintertime sea ice reduction of up to 58 % forecast for the end of the 21st century¹² and our 58 to 72 % decrease suggested for 128 ka. This implies that the 128 ka sea ice retreat may prove a crucial model-data target for the sea ice modelling community. Currently, the most recent Coupled Model Intercomparison Project Phase 5 multi-model simulations^{3,12,30} do not simulate a reduction in September sea ice area greater than 13 % between the LIG and the present interglacial (see Supplementary Discussion ). Considering the disagreement between modelled and observed Antarctic sea ice during the satellite era³¹, a number of studies have called for improvements in the modelling of climate and climate change in the Antarctic region³¹⁻³³. Whether this recent discrepancy is a function of natural variability³⁴ or represents a failing of current climate models is still a matter of debate³¹. If the currently observed increase in Antarctic sea ice is robust, a major reduction at 128 ka could indicate a tipping point in the sea ice system. There is clearly a need for more (and more robust) data for Antarctica and the surrounding sea ice edge during the LIG. If it is possible to correctly simulate the 128 ka sea ice reduction, it would improve the low confidence associated with future predictions of Southern Hemisphere sea ice change and, subsequently, improve projections of Antarctic temperature, precipitation and mass balance³⁵.

4 Methods

Ice core data. Four published ice core records from East Antarctica cover the LIG at a resolution of less than 200 years per m of ice¹⁶; Vostok³⁶, Dome F³⁷, EPICA Dome C (EDC)¹, and EPICA Dronning Maud Land (EDML)³⁸. Fractional isotopic content is expressed for oxygen-18 as: $\delta^{18}\text{O} = 1,000 \times [(\text{H}_2^{18}\text{O}/\text{H}_2^{16}\text{O})/\text{R}_{VSMOW} - 1]$ (in ‰), where R_{VSMOW} is the ratio of H_2^{18}O to H_2^{16}O for Vienna standard mean ocean water. The ice core isotope records are synchronised to the EDC3 age scale³⁹ and interpolated onto a common 100 year time grid using an interpolate point method. In order to minimise the effect of residual temporal misalignment between the ice cores, a 1,500 year low-pass filter is applied to each record before taking the LIG peak¹⁸. The misalignment and isotope measurement error is then assumed to be negligible after this averaging. The EDC3 age scale was chosen because the version of the EDML record corrected for upstream altitude changes and for the changing $\delta^{18}\text{O}$ of seawater is not available on the more recent AICC2012 age scale. However, as we are only interested in the LIG $\delta^{18}\text{O}$ maximum across ice core records, the choice of chronology does not have a significant influence on our results.



Isotope-enabled General Circulation Model (GCM) experiments. The isotope-enabled coupled General Circulation Model used in this study (HadCM3) has been tested for the present-day²⁰, the Last Glacial Maximum⁴⁰, as well as warm interglacials of the past^{40,41}. HadCM3 can be run for multi-millennial length simulations. The model has a reasonable representation of the global distribution of isotopes in the ocean and atmosphere^{20,41}. Among the Climate Model Intercomparison Project Phase 3 (CMIP3) model group, HadCM3 was assigned one of the highest skill scores based on global mean sea level pressure (mslp), sea surface temperature, height and temperature at 500 hPa, and surface mass balance over Antarctica⁴². The effect of seasonal biasing simulated by the HadCM3 model over Antarctica for the present day is similar to that calculated using the ECMWF ERA40 reanalysis product⁴³.

We use HadCM3 to simulate the isotopic response to differing West Antarctic Ice Sheet (WAIS) deglaciation scenarios and sea ice retreats during the LIG isotope maximum, 128,000 years ago (128 ka). We perform three suites of experiments, all forced with orbit and greenhouse gas values for 128 ka and compare to a pre-industrial control simulation, forced by 1850 yr BP orbit and greenhouse gas concentrations. The first suite uses a modern WAIS configuration, so the only difference from the control experiment are the 128 ka orbit and greenhouse gas forcing.

A second suite explores the isotopic response to WAIS deglaciation and includes experiments with; (i) a remnant WAIS with elevations reduced to 200 m and ice covered, following the approach of Holden *et al.* (2010)¹⁹; (ii) WAIS removed and replaced with a new region of ocean of 200 m depth; and (iii) as (ii) but with isotopically depleted meltwater from the WAIS added to the surface Southern Ocean. A prescribed freshwater flux of 0.4 Sv is added over a 100 year simulation (continued from the spun-up WAIS removed simulation), equivalent to a collapse of the WAIS and a global sea level contribution of 3.5 m. This can be considered an aggressive scenario and represents an idealised catastrophic collapse of the WAIS, such would be required by a very early complete loss of the WAIS during the LIG. The meltwater is distributed over the Southern Ocean according to current iceberg trajectories^{44,45}. The meltwater is added with an isotopic composition of -30 ‰, which is approximately equal to that of the parent ice sheet¹⁶. Apart from (iii), all experiments have been run for at least 700 years. This ensures that the upper ocean and atmosphere are in quasi-equilibrium with the respective boundary conditions. The new regions of ocean which are created when the WAIS is removed are allowed to evolve in the coupled simulation. No changes have been applied to the topography of the East Antarctic Ice Sheet (EAIS). This ensures we isolate the climate response to WAIS changes.

To investigate whether Southern Ocean sea ice retreat can provide an alternative explanation for the LIG isotope maximum, a third suite of experiments are performed using both the modern

WAIS configuration and with the WAIS removed and with a forced reduction in Antarctic sea ice extent. Each experiment is continued from the spun-up 128 ka modern WAIS and WAIS removed simulations and continued for an additional 50 years. We adopt a ‘clean’ method to force a sea ice retreat by prescribing a heat flux to the bottom of Antarctic sea ice at all longitudes and all latitudes south of 49 °S with no other effect to the model physics. The sea ice forcing is held constant throughout the annual cycle so the model can still calculate the seasonal cycle of sea ice growth and decay. Therefore, the simulated sea ice evolution is only reduced from the coupled models equilibrium response but still consistent with the internal model physics and sea surface temperatures and sea ice in our simulations are always internally consistent. The sea ice thus evolves with the coupled model, and the ocean and atmosphere respond to sea ice changes. We perform a range of experiments, each with a different prescribed heat flux from 0 W m⁻² (no forcing) up to 120 W m⁻² (see Supplementary Table 1 for a full list of experiments).

All modelled isotopic output is first re-gridded to an equal area 50 km grid and smoothed with the surrounding 100 km to remove grid dependence⁴³ before evaluation against ice core data. We calculate the simulated standard deviations, from annually resolved $\delta^{18}\text{O}$ model output, and those observed in the ‘raw’ ice core records (before being synchronised, placed on a common time scale and filtered; see previous section). Modelled and observed standard deviations for each of the four ice core sites (Vostok, Dome F, EDC and EDML) are 2.18, 2.70, 1.85 and 1.87 ‰, and 3.31, 2.12, 2.97 and 5.76 ‰ respectively. We also note reasonable agreement with results from a high resolution EPICA Dome C ice core record, describing the LIG on a 20 year resolution; suggesting a 3,000 year running mean standard deviation of 4.5 ‰⁴⁶.

Statistics. Inference about the sea ice retreat is conducted using the framework of Bayesian multivariate linear regression⁴⁷. A linear model is first fitted to the simulation outputs. $x^{(j)}$ denotes the input heat flux for the (j)th simulation, $y_i^{(j)}$ the vector of simulated annual average isotope

values at the four measurement sites in the (i) th equilibrium year of the (j) th simulation, and $z_i^{(j)}$ the corresponding sea ice retreat. Here, we use the term ‘equilibrium years’ to describe the model years after the surface ocean and atmosphere have reached a quasi-equilibrium with the input heat flux and the sea ice response has converged to a new steady state. The number of simulations is N , each of which has K equilibrium years.

The sea ice response reaches an equilibrium with the input heat flux within 20 years of each simulation so we use $K = 30$, i.e. we use the last 30 years from each 50 year sea ice forcing experiment for the following calculations. We include the experiments with heat fluxes of $[30, 35, 40, 45, 50, 60, 80]$, such that $N = 7$. The isotope and sea ice retreat values are modelled as jointly normally distributed with a linear dependence on the input heat flux,

$$\zeta_i^{(j)} \underset{\text{i.i.d.}}{\sim} \mathcal{N}(ax^{(j)} + b, \Sigma) \quad (3)$$

where $\zeta_i^{(j)}$ is a vector of all the dependent variables,

$$\zeta_i^{(j)} = \begin{bmatrix} y_i^{(j)} \\ z_i^{(j)} \end{bmatrix}, \quad (4)$$

and the unknown model parameters are the slope (a), intercept (b) covariance matrix (Σ). Note that a and b are 5-element column vectors with the first 4 elements corresponding to isotope measurements at the four sites and the fifth corresponding to the sea ice retreat. Σ is a 5×5 positive definite matrix. This can be written equivalently in matrix form using,

$$\theta = \begin{bmatrix} a & b \end{bmatrix}, \quad (5)$$

$$\tilde{x}^{(j)} = \begin{bmatrix} x^{(j)} \\ 1 \end{bmatrix}, \quad (6)$$

such that

$$ax^{(j)} + b = \theta \tilde{x}^{(j)}. \quad (7)$$

The complete sets of simulation variables will be written as

$$X = \{x^{(j)}\}_{j=1\dots N} \quad (8)$$

$$Z = \{\zeta_i^{(j)}\}_{i=1\dots K, j=1\dots N} \quad (9)$$

The model makes some strong assumptions about the temporal behaviour of the dependent variables. Over long time periods, climate variables are clearly not well modelled by a constant plus white noise, but display trends and seasonalities. However, over short intervals this simple equilibrium model can be sufficiently accurate. We checked for whiteness by testing all time series (those from the simulations and the equilibrium portions of the isotope records) with a Ljung-Box test⁴⁸, using 6 lags following the guideline of $K/5$ ⁴⁹, combining p-values using Fisher's method⁵⁰. There is no significant autocorrelation in the isotope measurements, but the simulation data for sea ice retreat does contain significant values for short lags. To remove this, we apply a preliminary whitening step. For this we model the raw data as the output of an autoregressive process of order 1 with unknown mean,

$$\widehat{z}_i^{(j)} = \mu^{(j)} + \gamma^{(j)}(\widehat{z}_{i-1}^{(j)} - \mu^{(j)}) + \epsilon_i^{(j)}, \quad (10)$$

where $\mu^{(j)}$ is the constant mean, and $\epsilon_i^{(j)}$ is an i.i.d. Gaussian perturbation. We can transform such a time series to an i.i.d. one using the following transformation,

$$z_i^{(j)} = \frac{\widehat{z}_i^{(j)} - \gamma^{(j)}\widehat{z}_i^{(j)}}{1 - \gamma^{(j)}} \quad (11)$$

$$= \mu^{(j)} + \frac{1}{1 - \gamma^{(j)}}\epsilon_i^{(j)}. \quad (12)$$

To do this, we first need to estimate $\gamma^{(j)}$, which can be achieved using a simple maximum likelihood procedure (jointly with $\mu^{(j)}$). This method allows us to remove temporal correlation, replacing it with an increased variance of each data point conditional on the preceding one. Full details can be found in the supporting iPython notebook.

We can write a probability density for the simulation variables conditional on the parameters,

$$p(Z|X, \theta, \Sigma) = \prod_{i,j} \left[|2\pi\Sigma|^{-\frac{1}{2}} \exp \left(-\frac{1}{2} (\zeta_i^{(j)} - \theta \tilde{x}^{(j)})^T \Sigma^{-1} (\zeta_i^{(j)} - \theta \tilde{x}^{(j)}) \right) \right] \quad (13)$$

$$= |2\pi\Sigma|^{-\frac{NK}{2}} \exp \left(-\frac{1}{2} \sum_{i,j} (\zeta_i^{(j)} - \theta \tilde{x}^{(j)})^T \Sigma^{-1} (\zeta_i^{(j)} - \theta \tilde{x}^{(j)}) \right). \quad (14)$$

In order to infer the values of the model parameters, we first assign them a conjugate prior, which is known to be a matrix normal-inverse Wishart distribution⁵¹,

$$p(\theta, \Sigma) = \mathcal{MN}(\theta|M_0, \Sigma, V_0) \mathcal{IW}(\Sigma|\nu_0, \Psi_0) \quad (15)$$

$$= |2\pi\Sigma|^{-\frac{c}{2}} |2\pi V_0|^{-\frac{d}{2}} \exp \left(-\frac{1}{2} \text{Tr} [(\theta - M_0)^T \Sigma^{-1} (\theta - M_0) V_0^{-1}] \right) \\ \times \frac{|\Psi_0|^{\frac{\nu_0}{2}}}{2^{\frac{\nu_0 d}{2}} \Gamma_d \left(\frac{\nu_0}{2} \right)} |\Sigma|^{-\frac{\nu_0 + d + 1}{2}} \exp \left(-\frac{1}{2} \text{Tr} [\Psi_0 \Sigma^{-1}] \right), \quad (16)$$

where $c \times d$ are the dimensions of θ , i.e. $c = 2$, $d = 5$, and M_0 , V_0 , ν_0 and Ψ_0 are hyperparameters to be specified. Since we have no particular prior information about the parameter values, we choose to make the prior uninformative. We obtain the Jeffreys prior by setting $\Psi_0 \rightarrow 0_{5 \times 5}$ (denoting the 5×5 matrix of zeros), $V_0^{-1} \rightarrow 0_{2 \times 2}$, and $\nu_0 \rightarrow 0^{52}$. (We could use a weakly informative prior to encode some basic deductions such as the fact that we expect a_z to be positive. However, since we have an informative likelihood function for this stage of the inference, the effect of such a prior is practically negligible.)

We can combine prior and likelihood to obtain a posterior distribution using Bayes' theorem,

$$p(\theta, \Sigma|X, Z) = \frac{p(Z|\theta, \Sigma, X) p(\theta, \Sigma)}{p(Z|X)}$$

$$\propto p(Z|X, \theta, \Sigma) p(\theta, \Sigma).$$



Note that we can ignore the denominator since it does not depend on θ or Σ . The unknown scale factor can be resolved by enforcing that the resulting probability distribution must integrate to 1.

Because we chose to use a conjugate prior, the posterior is also a matrix normal-inverse Wishart distribution⁵¹,

$$p(\theta, \Sigma | X, Z) = \mathcal{MN}(\theta | M, \Sigma, V) \mathcal{IW}(\Sigma | \nu, \Psi). \quad (17)$$

The updated hyperparameters are,

$$V^{-1} = K \sum_j \tilde{x}^{(j)} \tilde{x}^{(j)T} \quad (18)$$

$$M = \left(\sum_{i,j} \zeta_i^{(j)} \tilde{x}^{(j)T} \right) \left(K \sum_j \tilde{x}^{(j)} \tilde{x}^{(j)T} \right)^{-1} \quad (19)$$

$$\nu = NK \quad (20)$$

$$\Psi = \sum_{i,j} \zeta_i^{(j)} \zeta_i^{(j)T} - \left(\sum_{i,j} \zeta_i^{(j)} \tilde{x}^{(j)T} \right) \left(K \sum_j \tilde{x}^{(j)} \tilde{x}^{(j)T} \right)^{-1} \left(\sum_{i,j} \zeta_i^{(j)} \tilde{x}^{(j)T} \right)^T. \quad (21)$$

Note that the prior hyperparameters do not appear in these expressions because of our choice of the Jeffreys prior.

The model trained on the simulated data describes the distribution of annual isotope and sea ice retreat values. However, the ice core data does not provide annually resolved measurements. Furthermore the temporal resolution of the various ice cores is not the same, and there is likely to be some residual misalignment in the records even after the records have been synchronised. As stated above, we mitigate these effects by averaging the ice core isotope measurements over a selected interval of L years, where $L = 1500$. The chosen value of L represents an interval that is as large as possible while not compromising the assumption that the system is in a quasi-equilibrium.

We denote the average value of the dependent variables over the selected interval as $\bar{\zeta}$, such that,

$$\bar{\zeta} = \frac{1}{L} \sum_{i=1}^L \zeta_i, \quad (22)$$

where ζ_i now denotes the true values of the variables in a particular year. Since the annual values are assumed to be independent and identically distributed conditional on the linear model parameters, we then have,

$$p(\bar{\zeta}|x, \theta, \Sigma) = \mathcal{N}\left(\theta\tilde{x}, \frac{1}{L}\Sigma\right). \quad (23)$$

We assume that after this averaging step measurement error is negligible compared to the other sources of uncertainty.

For model comparison, we require the predicted distribution of the isotope measurements alone. This can be obtained by simple marginalisation. We partition $\bar{\zeta}$ and the parameter matrices into isotope and sea ice retreat components,

$$\bar{\zeta} = \begin{bmatrix} \bar{y} \\ \bar{z} \end{bmatrix} \quad (24)$$

$$\theta = \begin{bmatrix} \theta_y \\ \theta_z \end{bmatrix} = \begin{bmatrix} a_y & b_y \\ a_z & b_z \end{bmatrix}$$

$$\Sigma = \begin{bmatrix} \Sigma_{yy} & \Sigma_{yz} \\ \Sigma_{yz}^T & \Sigma_{zz} \end{bmatrix}. \quad (25)$$

Using standard Gaussian density identities, the predicted distribution for the isotope measurements is then simply⁴⁷,

$$p(\bar{y}|x, \theta, \Sigma) = \int p(\bar{\zeta}|x, \theta, \Sigma) d\bar{z} \quad (26)$$

$$= \mathcal{N}\left(\theta_y\tilde{x}, \frac{1}{L}\Sigma_{yy}\right). \quad (27)$$

Using this basic formulation, models trained on the with-WAIS and without-WAIS simulation data both assign very small likelihoods to the measured isotope values. The problem is that

neither model predicts the isotope measurements to within the expected accuracy, since both are imperfect representations of the real system. However we can still assess which is better by incorporating this error into the analysis. To this end, the observed vector of isotopes \tilde{y} is modelled as the predicted value plus some error term, such that,

$$p(\tilde{y}|\bar{y}, \sigma_e^2) = \mathcal{N}(\tilde{y}|\bar{y}, \sigma_e^2 I_{4 \times 4}), \quad (28)$$

where $I_{4 \times 4}$ is the 4×4 identity matrix. Hence,

$$p(\tilde{y}|x, \theta, \Sigma, \sigma_e^2) = \int p(\tilde{y}|\bar{y}, \sigma_e^2) p(\bar{y}|x, \theta, \Sigma) d\bar{y} \quad (29)$$

$$= \mathcal{N}\left(\tilde{y} \middle| \theta_y \tilde{x}, \frac{1}{L} \Sigma_{yy} + \sigma_e^2 I_{4 \times 4}\right). \quad (30)$$

Hypothesis Testing. The standard mechanism for comparing two statistical models is to compute the marginal likelihood (also known as the model evidence) for each⁴⁷. This is the probability assigned to the observed data by the model, averaging over all possible model parameter values,

$$p(\tilde{y}) = \int p(\tilde{y}, x, \sigma_e | \theta, \Sigma) p(\theta, \Sigma | X, Z) dx d\sigma_e d\theta d\Sigma \quad (31)$$

$$= \int p(\tilde{y}|x, \sigma_e, \theta, \Sigma) p(x, \sigma_e | \theta, \Sigma) p(\theta, \Sigma | X, Z) dx d\sigma_e d\theta d\Sigma. \quad (32)$$

This cannot be evaluated analytically, so instead we approximate it numerically. The linear model parameter integrals are handled with Monte Carlo sampling. The remaining integrals over the heat flux and error scale variables may be handled using an Empirical Bayes evidence approximation. Since the posterior distribution for these variables is sharply peaked, the prior probability density may be replaced with a point mass at the maximum likelihood value⁴⁷,

$$p(x, \sigma_e | \theta, \Sigma) = \delta_{\hat{x}(\tilde{y}, \theta, \Sigma), \hat{\sigma}_e(\tilde{y}, \theta, \Sigma)}(x, \sigma_e), \quad (33)$$

where,

$$\hat{x}(\tilde{y}, \theta, \Sigma), \hat{\sigma}_e(\tilde{y}, \theta, \Sigma) = \underset{x, \sigma_e}{\operatorname{argmax}} : p(\tilde{y}|x, \sigma_e, \theta, \Sigma). \quad (34)$$

This also removes the necessity of specifying a prior distribution over x and σ_e . Applying the two approximations, we obtain,

$$p(\tilde{y}) \approx \frac{1}{M} \sum_{m=1}^M p(\tilde{y}|\hat{x}(\tilde{y}, \theta^{[m]}, \Sigma^{[m]}), \hat{\sigma}_e(\tilde{y}, \theta^{[m]}, \Sigma^{[m]}), \theta^{[m]}, \Sigma^{[m]}) \quad (35)$$

$$= \frac{1}{M} \sum_{m=1}^M \mathcal{N}\left(\tilde{y} \left| a_y^{[m]} \hat{x}(\tilde{y}, \theta^{[m]}, \Sigma^{[m]}) + b_y^{[m]}, \frac{1}{L} \Sigma_{yy}^{[m]} + \hat{\sigma}_e(\tilde{y}, \theta^{[m]}, \Sigma^{[m]})^2 I \right.\right) \quad (36)$$

where $\theta^{[m]}, \Sigma^{[m]}$ are sampled values of the linear model parameters drawn from the fitted posterior distribution. In our calculations we used 1,000 Monte Carlo samples.

The average maximum likelihood values for heat flux are 72 W/m^2 and 51 W/m^2 respectively for the with-WAIS and without-WAIS models. Comparing the two scenarios, the likelihood ratio is 200 in favour of the WAIS being present (quoted to one significant figure), i.e. the observed data is 200 times more likely using a model with the WAIS present than when the WAIS is removed. Moreover, the average error scale for the with-WAIS model is 0.6 ‰ , compared with 1.9 ‰ for the without-WAIS model, indicating that larger error terms are needed in combination with the without-WAIS model to obtain the most likely system. These results strongly support the conclusion that the with-WAIS model is a more accurate representation of the ice core data. For the two scenarios, the probability of the with-WAIS model is 99.5 ‰ .

Calculating the Sea Ice Retreat. Taking into account the isotope measurements, knowledge

about the corresponding average sea ice retreat is conveyed by the posterior distribution,

$$p(\bar{z}|\tilde{y}) \propto p(\bar{z}, \tilde{y}) \quad (37)$$

$$= \int p(\bar{z}, \tilde{y}, x, \sigma_e | \theta, \Sigma) p(\theta, \Sigma | X, Z) dx d\sigma_e d\theta d\Sigma \quad (38)$$

$$= \int p(\bar{z}, \tilde{y} | x, \sigma_e, \theta, \Sigma) p(x, \sigma_e | \theta, \Sigma) p(\theta, \Sigma | X, Z) dx d\sigma_e d\theta d\Sigma. \quad (39)$$

This is the probability distribution over the possible values for sea ice retreat conditional on the particular observed isotope measurements, but averaging over the possible values for the model parameters. As before, the integrals cannot be evaluated analytically, and numerical methods must be used.

Starting with the joint probability distribution over isotope and sea ice retreat, and applying the Monte Carlo and Empirical Bayes approximations as before, we obtain,

$$p(\bar{z}, \tilde{y}) \approx \frac{1}{M} \sum_{m=1}^M p(\bar{z}, \tilde{y} | \hat{x}(\tilde{y}, \theta^{[m]}, \Sigma^{[m]}), \hat{\sigma}_e(\tilde{y}, \theta^{[m]}, \Sigma^{[m]}), \theta^{[m]}, \Sigma^{[m]}) \quad (40)$$

$$= \frac{1}{M} \sum_{m=1}^M \mathcal{N} \left(\begin{bmatrix} \tilde{y} \\ \bar{z} \end{bmatrix} \middle| \begin{bmatrix} a_y^{[m]} \hat{x}(\tilde{y}, \theta^{[m]}, \Sigma^{[m]}) + b_y^{[m]} \\ a_z^{[m]} \hat{x}(\tilde{y}, \theta^{[m]}, \Sigma^{[m]}) + b_z^{[m]} \end{bmatrix}, \begin{bmatrix} \frac{1}{L} \Sigma_{yy}^{[m]} + \hat{\sigma}_e(\tilde{y}, \theta^{[m]}, \Sigma^{[m]})^2 I & \frac{1}{L} \Sigma_{yz}^{[m]} \\ \frac{1}{L} \Sigma_{yz}^{[m]T} & \frac{1}{L} \Sigma_{zz}^{[m]} \end{bmatrix} \right). \quad (41)$$

Finally, conditioning on the isotope measurements using standard Gaussian density identities⁴⁷, the posterior distribution is approximated by,

$$p(\bar{z}|\tilde{y}, \theta, \Sigma) \approx \frac{1}{M} \sum_{m=1}^M \mathcal{N}(\bar{z} | \tilde{\alpha}^{[m]}, \tilde{\beta}^{[m]}), \quad (42)$$

where,

$$\begin{aligned} \tilde{\alpha}^{[m]} &= a_z^{[m]} \hat{x}(\tilde{y}, \theta^{[m]}, \Sigma^{[m]}) + b_z^{[m]} + \left(\frac{1}{L} \Sigma_{yz}^{[m]} \right)^T \\ &\quad \left(\frac{1}{L} \Sigma_{yy}^{[m]} + \hat{\sigma}_e(\tilde{y}, \theta^{[m]}, \Sigma^{[m]})^2 I \right)^{-1} (\tilde{y} - a_y^{[m]} \hat{x}(\tilde{y}, \theta^{[m]}, \Sigma^{[m]}) - b_y^{[m]}) \end{aligned} \quad (43)$$

$$\tilde{\beta}^{[m]} = \frac{1}{L} \Sigma_{zz}^{[m]} - \left(\frac{1}{L} \Sigma_{yz}^{[m]} \right)^T \left(\frac{1}{L} \Sigma_{yy}^{[m]} + \hat{\sigma}_e(\tilde{y}, \theta^{[m]}, \Sigma^{[m]})^2 I \right)^{-1} \left(\frac{1}{L} \Sigma_{yz}^{[m]} \right). \quad (44)$$

Our final approximation of the distribution is a Gaussian mixture, from which a mean value and credible intervals may be obtained. This provides us with the distribution of the average sea ice retreat over the L years in our window. There is an additional uncertainty of $\left[1 - \frac{1}{L}\right] \Sigma_{zz}$ associated with each individual year due to the random annual variation.

For the with-WAIS scenario, we estimate the sea ice retreat during the LIG isotope maximum to be 65 % (posterior mean). For the sea ice retreat in an arbitrary year, the 95 % credible interval is [58 %, 72 %]. For the average value of sea ice retreat over the 1500 year period considered, the 95 % credible interval is [61 %, 70 %]. For the without-WAIS model, the same calculation similarly suggests an estimated best fit sea ice retreat to fit the observations during the LIG isotope maximum of 66 % (posterior mean). However, the uncertainty band is more than three times larger than for the with-WAIS scenario. For the sea ice retreat in an arbitrary year, the 95 % credible interval is [32 %, 87 %]. For the average value of sea ice retreat over the 1500 year period considered, the 95 % credible interval is [32 %, 86 %]. In the main text of the manuscript we quote the posterior mean and the credibility interval for an arbitrary year during the 1,500 year period spanning the LIG isotope maximum for each scenario.

1. Jouzel, J. *et al.* Orbital and millennial Antarctic climate variability over the past 800,000 years. *Science* **317**, 793–796 (2007).
2. Otto-Bliesner, B. L. *et al.* How warm was the last interglacial? New model-data comparisons. *Philosophical Transactions of The Royal Society A* **371** (2013).
3. Bakker, P. *et al.* Temperature trends during the Present and Last Interglacial periods - a multi-model-data comparison. *Quaternary Science Reviews* **99**, 224–243 (2014).

4. Capron, E. *et al.* Temporal and spatial structure of multi-millennial temperature changes at high latitudes during the Last Interglacial. *Quaternary Science Reviews* **103**, 116–133 (2014).
5. Dahl-Jensen, D. *et al.* Eemian interglacial reconstructed from a Greenland folded ice core. *Nature* **493**, 489–94 (2013).
6. Dutton, A., Webster, J. M., Zwartz, D., Lambeck, K. & Wohlfarth, B. Tropical tales of polar ice: Evidence of Last Interglacial polar ice sheet retreat recorded by fossil reefs of the granitic Seychelles islands. *Quaternary Science Reviews* **107**, 182–196 (2015).
7. Kopp, R. E., Simons, F. J., Mitrovica, J. X., Maloof, A. C. & Oppenheimer, M. Probabilistic assessment of sea level during the last interglacial stage. *Nature* **462**, 863–867 (2009).
8. Kopp, R. E., Simons, F. J., Mitrovica, J. X., Maloof, a. C. & Oppenheimer, M. A probabilistic assessment of sea level variations within the last interglacial stage. *Geophysical Journal International* **193**, 711–716 (2013).
9. O’Leary, M. J. *et al.* Ice sheet collapse following a prolonged period of stable sea level during the last interglacial. *Nature Geoscience* **6**, 1–5 (2013).
10. Grant, K. *et al.* Rapid coupling between ice volume and polar temperature over the past 150,000 years. *Nature* **491**, 744–747 (2012).
11. Dutton, A. *et al.* Sea-level rise due to polar ice-sheet mass loss during past warm periods. *Science* **349** (2015).
12. IPCC. *Climate Change 2013: The Physical Science Basis. Contribution of Working Group I to the Fifth Assessment Report of the Intergovernmental Panel on Climate Change* (Cambridge University Press, Cambridge, United Kingdom and New York, NY, USA, 2013).
13. Joughin, I. & Alley, R. B. Stability of the West Antarctic ice sheet in a warming world. *Nature Geoscience* **4**, 506–513 (2011).

14. Bamber, J. L., Riva, R. E. M., Vermeersen, B. L. A. & LeBrocq, A. M. Reassessment of the potential sea-level rise from a collapse of the West Antarctic Ice Sheet. *Science* **324**, 901–903 (2009).
15. WAIS Divide Project Members. Onset of deglacial warming in West Antarctica driven by local orbital forcing. *Nature* **6** (2013).
16. Masson-Delmotte, V. *et al.* A comparison of the present and last interglacial periods in six Antarctic ice cores. *Climate of the Past* **7**, 397–423 (2011).
17. Stenni, B. *et al.* The deuterium excess records of EPICA Dome C and Dronning Maud Land ice cores (East Antarctica). *Quaternary Science Reviews* **29**, 146–159 (2010).
18. Sime, L. C., Wolff, E. W., Oliver, K. I. C. & Tindall, J. C. Evidence for warmer interglacials in East Antarctic ice cores. *Nature* **462**, 342–345 (2009).
19. Holden, P. B. *et al.* Interhemispheric coupling, the West Antarctic Ice Sheet and warm Antarctic interglacials. *Climate of the Past* **6**, 431–443 (2010).
20. Tindall, J. C., Valdes, P. J. & Sime, L. C. Stable water isotopes in HadCM3: Isotopic signature of El Niño-Southern Oscillation and the tropical amount effect. *Journal of Geophysical Research* **114**, 12pp. (2009).
21. Noone, D. & Simmonds, I. Sea ice control of water isotope transport to Antarctica and implications for ice core interpretation. *Journal of Geophysical Research* **109**, 13pp. (2004).
22. Wolff, E. *et al.* Changes in environment over the last 800,000 years from chemical analysis of the EPICA Dome C ice core. *Quaternary Science Reviews* **29**, 285–295 (2010).
23. Fischer, H. *et al.* Reconstruction of millennial changes in dust emission, transport and regional sea ice coverage using the deep EPICA ice cores from the Atlantic and Indian Ocean sector of Antarctica. *Earth and Planetary Science Letters* **260**, 340–354 (2007).

24. Bianchi, C. & Gersonde, R. The Southern Ocean surface between Marine Isotope Stages 6 and 5d: Shape and timing of climate changes. *Palaeogeography, Palaeoclimatology, Palaeoecology* **187**, 151–177 (2002).
25. Liu, X. & Battisti, D. S. The Influence of Orbital Forcing of Tropical Insolation on the Climate and Isotopic Composition of Precipitation in South America. *Journal of Climate* **28**, 4841–4862 (2015).
26. Walsh, K. J. E., Simmonds, I. & Collier, M. Sigma-coordinate calculation of topographically forced baroclinicity around Antarctica. *Dynamics of Atmospheres and Oceans* **33**, 1–29 (2000).
27. Steig, E. J. *et al.* Influence of West Antarctic Ice Sheet collapse on Antarctic surface climate. *Geophysical Research Letters* **42**, 4862–4868 (2015).
28. Stocker, T. F. & Johnsen, S. J. A minimum thermodynamic model for the bipolar seesaw. *Paleoceanography* **18** (2003).
29. Marino, G. *et al.* Bipolar seesaw control on last interglacial sea level. *Nature* **522**, 197–201 (2015).
30. Lunt, D. J. *et al.* A multi-model assessment of last interglacial temperatures. *Climate of the Past* **9**, 699–717 (2013).
31. Simmonds, I. Comparing and contrasting the behaviour of Arctic and Antarctic sea ice over the 35 year period 1979–2013. *Annals of Glaciology* **56**, 18–28 (2015).
32. Turner, J., Bracegirdle, T., Phillips, T., Marshall, G. J. & Hosking, J. S. An Initial Assessment of Antarctic Sea Ice Extent in the CMIP5 Models. *Journal of Climate* **26**, 1473–1484 (2013).

33. Zunz, V., Goosse, H. & Massonnet, F. How does internal variability influence the ability of CMIP5 models to reproduce the recent trend in Southern Ocean sea ice extent? *The Cryosphere* **7**, 451–468 (2013).
34. Kohyama, T. & Hartmann, D. L. Antarctic sea ice response to weather and climate modes of variability. *Journal of Climate* **29**, 721–741 (2016).
35. Bracegirdle, T. J., Stephenson, D. B., Turner, J. & Phillips, T. The importance of sea-ice area biases in 21 st century multi-model projections of Antarctic temperature and precipitation. *Geophysical Research Letters* **42**, 10,832–10,839 (2015).
36. Petit, J. R. *et al.* Climate and atmospheric history of the past 420,000 years from the Vostok ice core, Antarctica. *Nature* **399**, 429–413 (1999).
37. Kawamura, K. *et al.* Northern Hemisphere forcing of climatic cycles in Antarctica over the past 360,000 years. *Nature* **448**, 912–916 (2007).
38. EPICA Community Members. One-to-one coupling of glacial climate variability in Greenland and Antarctica. *Nature* **444**, 195–198 (2006).
39. Parrenin, F. *et al.* The EDC3 chronology for the EPICA Dome C ice core. *Climate of the Past* **3**, 485–497 (2007).
40. Holloway, M. D., Sime, L. C., Singarayer, J. S., Tindall, J. C. & Valdes, P. J. Reconstructing paleosalinity from $\delta^{18}\text{O}$: Coupled model simulations of the Last Glacial Maximum, Last Interglacial and Late Holocene. *Quaternary Science Reviews* **131**, 350–364 (2016).
41. Tindall, J. *et al.* Modelling the oxygen isotope distribution of ancient seawater using a coupled ocean-atmosphere GCM: Implications for reconstructing early Eocene climate. *Earth and Planetary Science Letters* **292**, 265–273 (2010).

42. Connolley, W. M. & Bracegirdle, T. J. An Antarctic assessment of IPCC AR4 coupled models. *Geophysical Research Letters* **34**, 1–6 (2007).
43. Sime, L. C., Tindall, J. C., Wolff, E. W., Connolley, W. M. & Valdes, P. J. Antarctic isotopic thermometer during a CO₂ forced warming event. *Journal of Geophysical Research* **113** (2008).
44. Gladstone, R. M., Bigg, G. R. & Nicholls, K. W. Iceberg trajectory modeling and meltwater injection in the Southern Ocean. *Journal of Geophysical Research* **106**, 19903–19915 (2001).
45. Jacobs, S. Observations of change in the Southern Ocean. *Philosophical Transactions of the Royal Society A: Mathematical, Physical and Engineering Sciences* **364**, 1657–1681 (2006).
46. Pol, K. *et al.* Climate variability features of the last interglacial in the East Antarctic EPICA Dome C ice core. *Geophysical Research Letters* **41**, 4004–4012 (2014).
47. Bishop, C. M. *Pattern Recognition and Machine Learning (Information Science and Statistics)* (Springer-Verlag New York, Inc., Secaucus, NJ, USA, 2006).
48. Ljung, G. M. & Box, G. E. P. On a measure of lack of fit in time series models. *Biometrika* **65**, 297–303 (1978).
49. Hyndman, R. J. & Athanasopoulos, G. *Forecasting: principles and practice* (OTexts, 2014).
50. Fisher, R. A. *Statistical Methods For Research Workers*. Cosmo study guides (Cosmo Publications, 1925).
51. Box, G. E. P. & Tiao, G. C. *Bayesian inference in statistical analysis*. Addison-Wesley series in behavioral science: quantitative methods (Addison-Wesley Pub. Co., 1973).
52. Yang, R. & Berger, J. O. Estimation of a Covariance Matrix Using the Reference Prior. *The Annals of Statistics* **22**, 1195–1211 (1994).

End Notes

Acknowledgements

We thank Pepijn Bakker for supplying sea ice model output from a selection of PMIP3 models covering the LIG, Peter Hopcroft for his advice on sea ice forcing, and Eric Wolff for constructive discussion. We thank the four reviewers for their constructive comments, which helped improved the manuscript through the review process. M.D.H. is supported by a NERC studentship tied between the British Antarctic Survey and the University of Bristol. The work was partially funded by NERC grant NE/J004804/1, and also forms part of the British Antarctic Survey Polar Science for Planet Earth Programme. J.C.T. has received funding from the European Research Council under the European Union's Seventh Framework Programme (FP7/2007-2013)/ERC grant number 278636. The climate model simulations were carried out using the computational facilities of the Advanced Computing Research Centre, University of Bristol (<http://www.bris.ac.uk/acrc/>) and the ARCHER UK National Supercomputing Service (<http://www.archer.ac.uk>).

Author Contribution

M.D.H. undertook the climate model simulations, performed the analysis and wrote the manuscript. P.B. developed the statistical methods. L.C.S. and J.S.S. provided the initial motivation for the work. L.C.S. provided feedback throughout the analysis and writing. J.C.T. and P.J.V. provided additional technical advice related to running and interpreting the isotope-enabled climate model simulations. All authors discussed the results and commented on the manuscript. The authors confirm that there are no conflicts of interest.

Figure legends


Fig. 1. Time series of Antarctic ice core stable water isotope records and sea level during the last interglacial. (a) Stable water isotope ($\delta^{18}\text{O}$ and δD) anomalies relative to the last 3 ka from four deep ice cores¹⁶; EPICA Dronning Maud Land (EDML; green)  Dome F (DF; red), Vostok (blue), and EPICA Dome C (EDC; orange for δD and purple for $\delta^{18}\text{O}$). (b) Global sea level⁷ (purple curve; heavy line marks median projection, dashed lines the 16th and 84th percentiles, dotted lines the 2.5th and 97.5th percentiles) and Red Sea relative sea level¹⁰ records (brown curve; solid line shows maximum likelihood and shading represents 95 % confidence limits). The Antarctic isotope peak at 128 ± 2 ka is shaded grey.

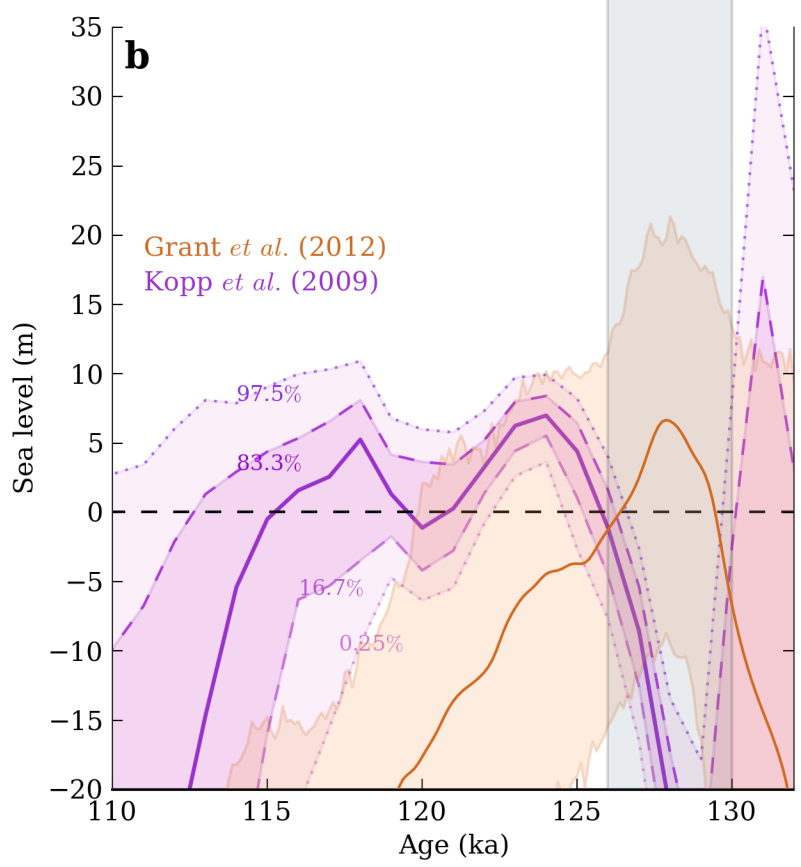
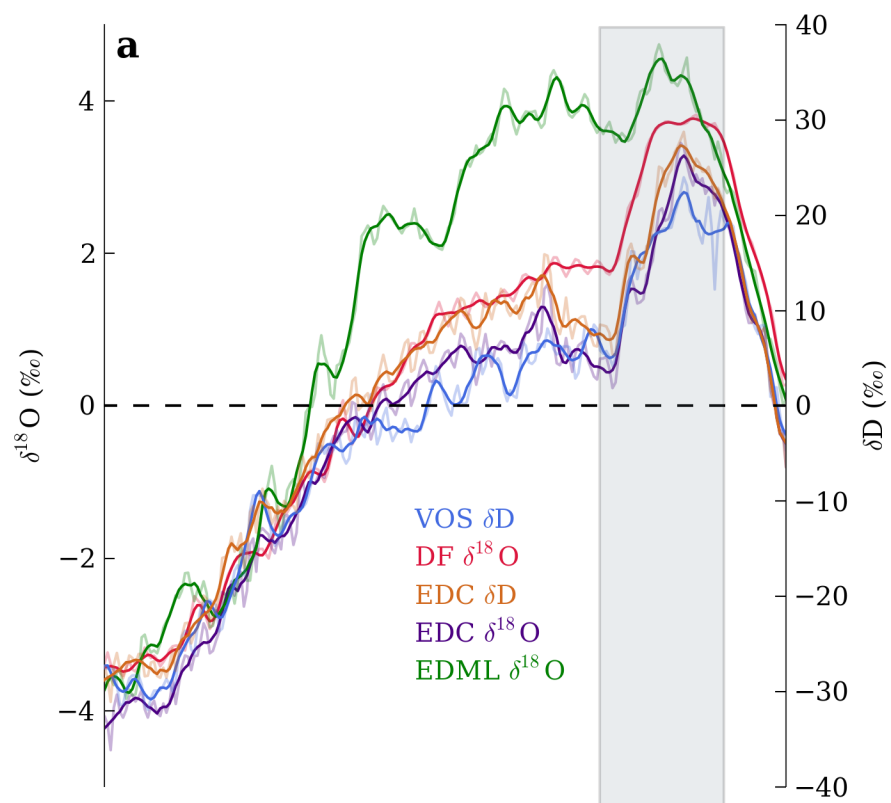
Fig. 2. Spatial pattern of $\delta^{18}\text{O}$ anomalies. Precipitation weighted $\delta^{18}\text{O}$ anomalies (LIG-PI) for 128 ka simulations with (a) a modern WAIS configuration, (b) the WAIS flattened (indicated by stippling), (c) the WAIS removed and replaced with a new region of ocean (indicated by crosshatching), and (d) the WAIS removed and meltwater added to the Southern Ocean. Filled circles show ice core $\delta^{18}\text{O}$ anomalies for the LIG maximum at approximately 128 ka (see Methods). Grey lines signify the 15 % September sea ice concentration threshold.

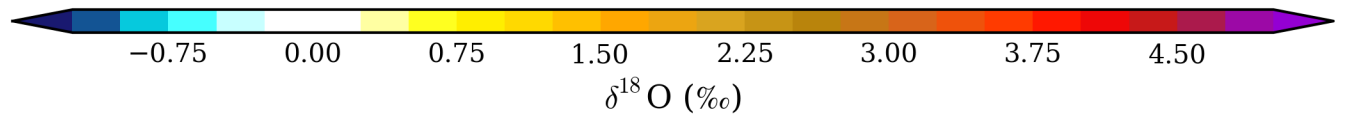
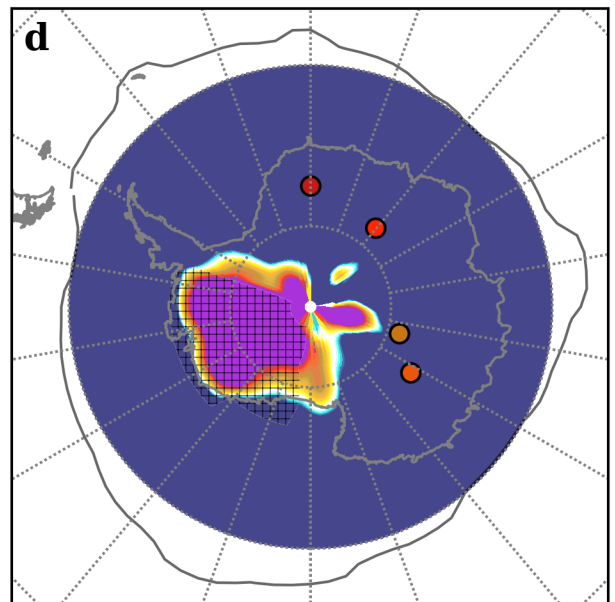
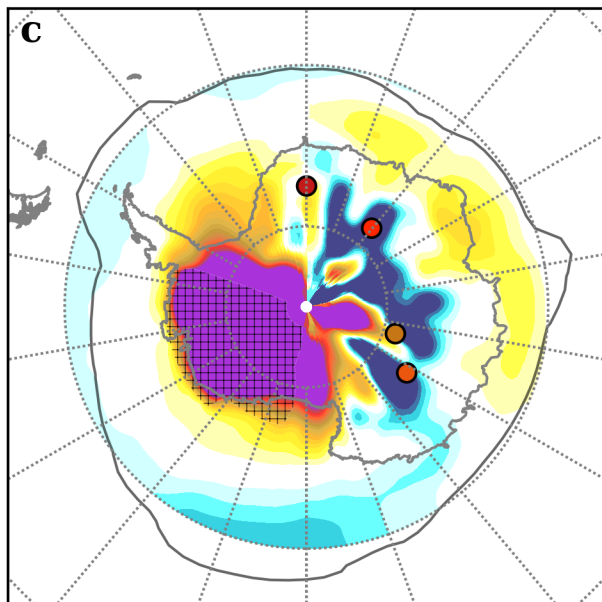
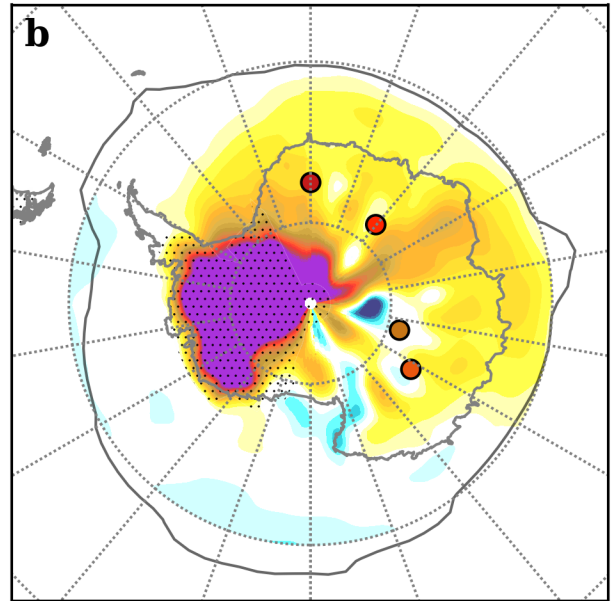
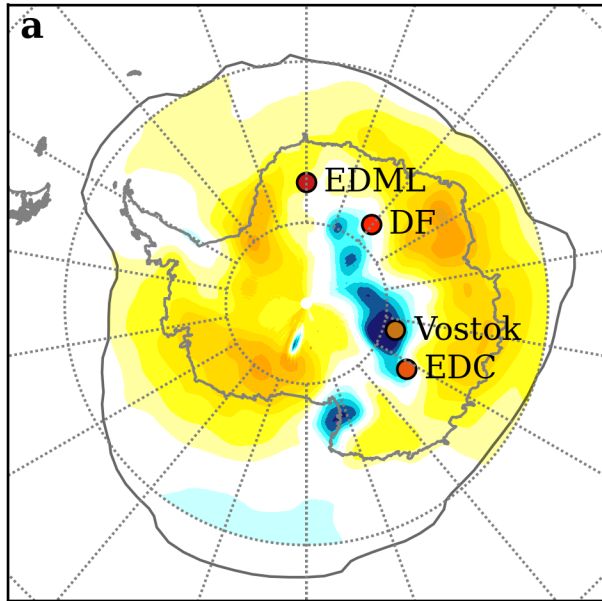
Fig. 3. Decomposition of $\delta^{18}\text{O}$ anomalies from 128 ka WAIS retreat experiments. (a-c); A remnant flat WAIS, (d-f); WAIS removed and replaced with ocean, (g-i); WAIS removed and meltwater added to the surface Southern Ocean. Left panels (a,d,g); the total $\delta^{18}\text{O}$ change between experiments ($\Delta\delta^{18}\text{O}$). Middle panels (b,e,h); the change due to changes in the seasonal cycle of precipitation (ΔP_{seas}). Right panels (c,f,i); the change due to other effects, such as the monthly isotopic composition of precipitation ($\Delta\delta$). Anomalies are calculated relative to a 128 ka experiment using a modern WAIS configuration. This calculation was performed using isotopic output

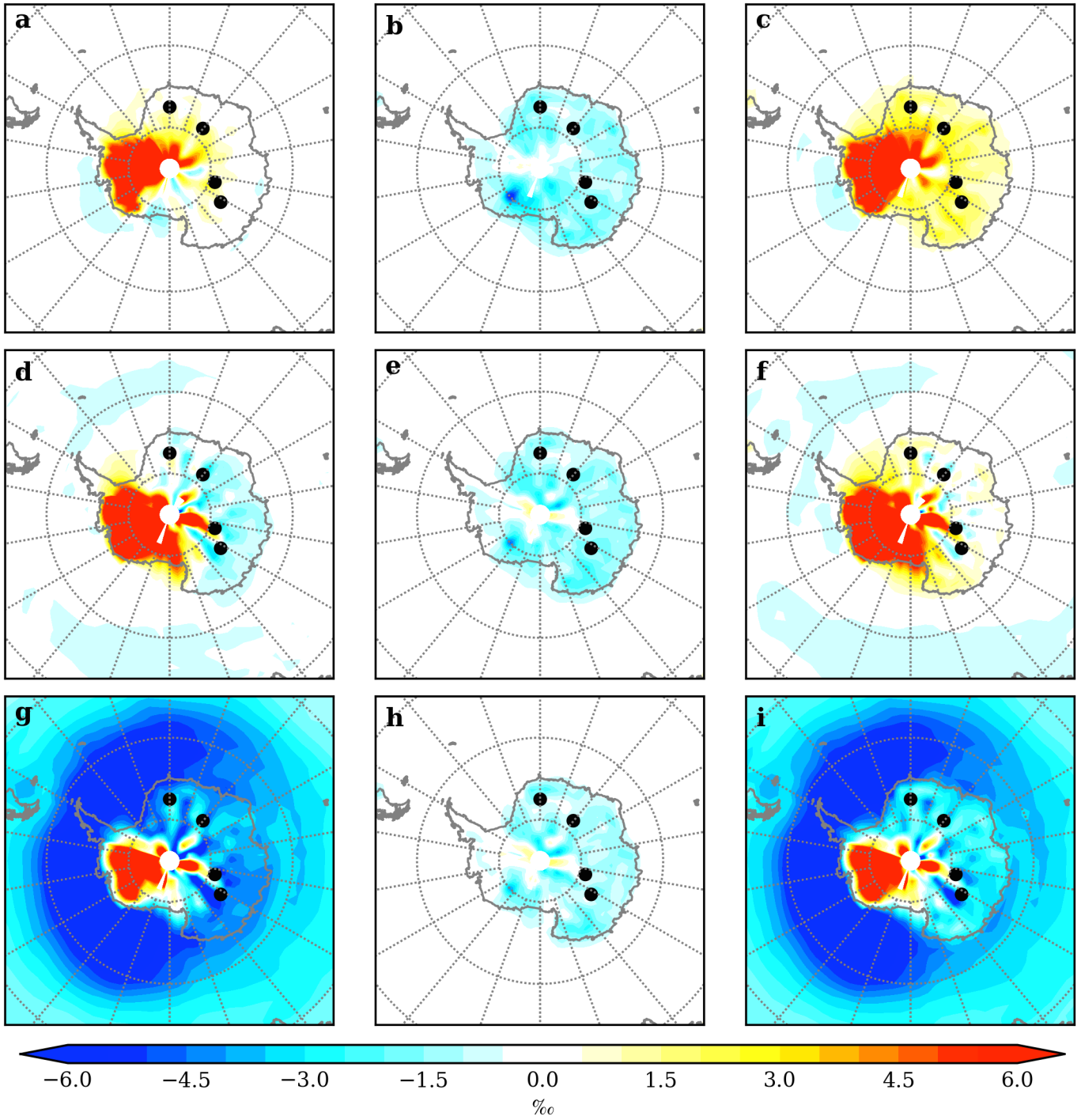
from the native model grid, with no re-gridding, due to the need for monthly resolved data.

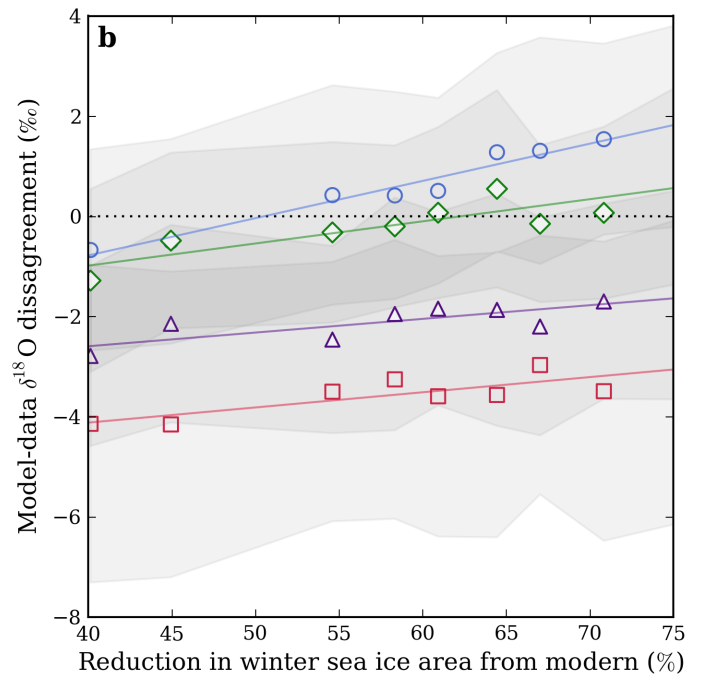
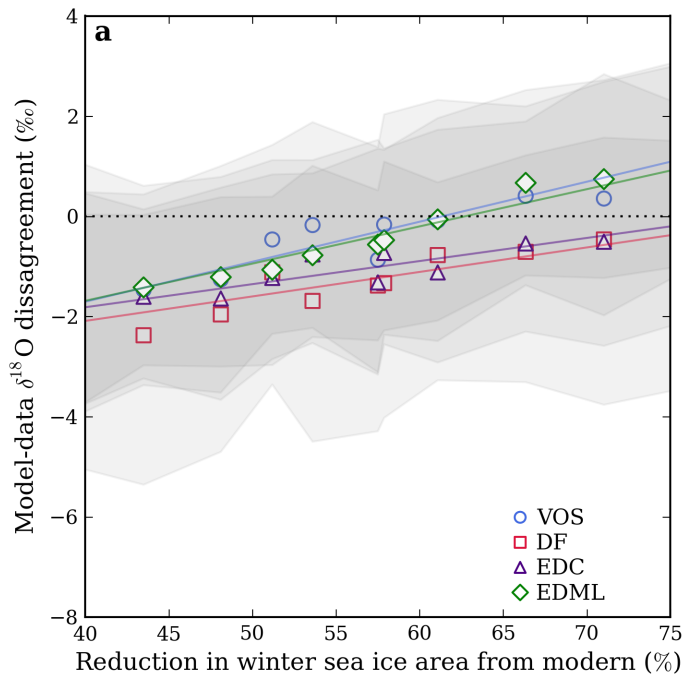
Fig. 4. Model-data $\delta^{18}\text{O}$ match at ice core sites. Ice core sites shown include Vostok (VOS; blue circles), Dome F (DF; red squares), EDC (purple triangles), and EDML (green diamonds). Results shown for sea ice retreat experiments and (a) a modern WAIS configuration and (b) with the WAIS removed and replaced with ocean. Sea ice retreat is measured as the percentage change in winter (September) sea ice area, relative to the pre-industrial control experiment. Shaded envelopes signify one standard deviation on simulated annual $\delta^{18}\text{O}$ at each site. Best fit lines have been added to each site (coloured as above).

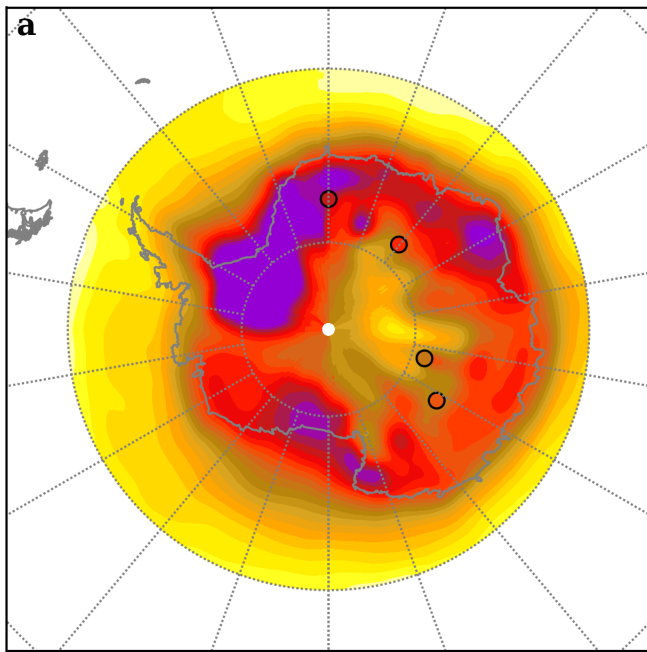
Fig. 5. Spatial pattern of $\delta^{18}\text{O}$ anomalies for the best fit sea ice retreat. Precipitation weighted $\delta^{18}\text{O}$ anomalies (LIG-PI) interpolated between 128 ka experiments to best fit the ice core LIG maximum, corresponding to a 65 % winter sea ice retreat relative to pre-industrial. (b) September sea ice concentration (sic) fraction, corresponding to (a). Black contour signifies the simulated 15 % September sea ice concentration threshold. Blue contour signifies 1978-2013 satellite observations.



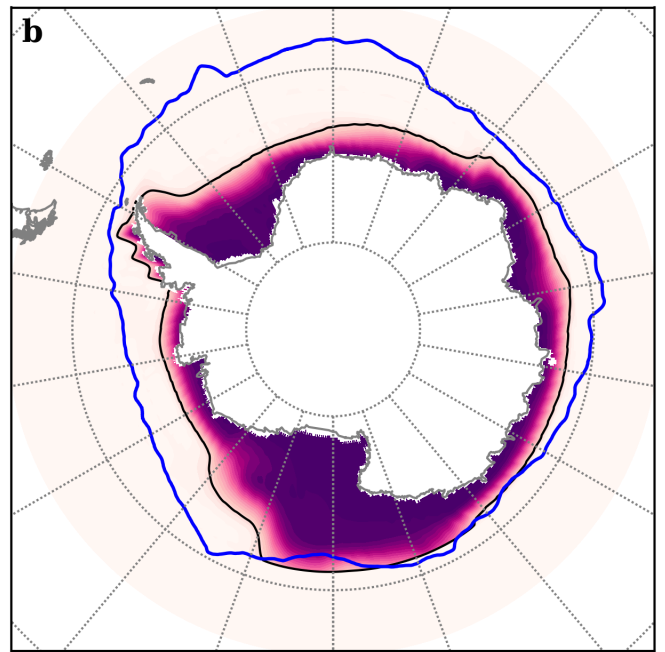








-0.75 0.00 0.75 1.50 2.25 3.00 3.75 4.50
 $\delta^{18}\text{O}$ (‰)



0.0 0.1 0.2 0.3 0.4 0.5 0.6 0.7 0.8 0.9
sic (fraction)